DIELECTRIC PROPERTIES OF PURE $Y_{2/3}Cu_3Ti_4O_{12}$ SYNTHESIZED BY SEMI-WET ROUTE

CHAPTER 3

3.1 INTRODUCTION

Materials with high dielectric constant find application in micro-capacitors required for integrated circuits. Traditional $BaTiO_3$-based ferroelectric materials are well-known as high dielectric constant materials. But the major problem with these materials is the strong dependence of their dielectric constant on temperature near ferroelectric to paraelectric transition, quite undesirable from the device point of view (Chou *et al.*, 2007; Zhao *et al.*, 2007). A Family of $ACu_3Ti_4O_{12}$ compounds has been studied based upon microstructure and dielectric properties since its discovery (Deschanvres *et al.*, 1967). The complex perovskite-based $ACu_3Ti_4O_{12}$ (A = Ca, $Bi_{2/3}$, $Y_{2/3}$) materials also possess high dielectric constant. They could be promising candidates to replace relaxors as dielectrics in DRAM, MLCCs and other memory devices (Hongtao *et al.*, 2000). Their smaller capacitive components lead to miniaturization of electronic devices with efficient performance. Such materials could be technically significant for introducing the state of the art in semiconductor integrated circuits (ICs) owing to their high reliability, high integration potential, good dielectric properties and excellent thermal conductivity as their thermal expansion coefficient close to silicon (Moulson *et al.*, 2003). One of the ceramics, $CaCu_3Ti_4O_{12}$ (CCTO), has been studied for the last one decade owing to its giant dielectric constant ($\varepsilon \sim 10^4$ for bulk and 10^5 for single crystal). The dielectric constant of CCTO remains independent of temperature (100 – 600 K) and frequency (10^2-10^6 Hz) (Subramanian *et al.*, 2000). Such behaviour of CCTO is technically attractive to the development of future electronic devices. However, in contrast to regular ferroelectric like $BaTiO_3$, CCTO does not exhibit any ferroelectric transition as observed in other perovskites. Recently, it has been reported that the dielectric properties of CCTO are mainly influenced by factors like methods of processing,

sintering time, sintering temperature, doping schemes as well as nature of dopants and their stoichiometric variations (Li *et al.*, 2008; Rai *et al.*, 2009). The mystery of the origin of giant dielectric constant in CCTO ceramic has been explained in terms of internal barrier layer capacitor (IBLC) effects originating due to semiconducting grains with insulating grain boundaries. This mechanism has been widely accepted, though it is still controversial.

Various isostructural materials based on complex perovskite structure, like $ACu_3Ti_4O_{12}$ (A = $Y_{2/3}$, $Bi_{2/3}$, $La_{2/3}$, $Nd_{2/3}$, $Sm_{2/3}$, $Gd_{2/3}$, $Dy_{2/3}$) also exhibit similar dielectric properties with excellent thermal stability (Homes *et al.*, 2001; Liu *et al.*, 2005). Apart from this, a wide variety of doping or partial substitution may be carried out at A, Cu or Ti-site of $ACu_3Ti_4O_{12}$. The choice of the substituent to modify the physical properties of the material is based on many factors including tolerance factor, ionic radius, charge neutrality and solubility. The partial isovalent substitution of metal cations in different interstices can improve properties associated with ferroelectricity and dielectric response in these materials through partial modification of mixed-valent structure. Further, structural flexibility and chemical versatility of the materials could make them more suitable for device applications. It is quite inspiring to investigate systematically new $ACu_3Ti_4O_{12}$ like materials possessing temperature independent high dielectric constant and low dielectric loss with excellent thermal stability.

$Y_{2/3}Cu_3Ti_4O_{12}$ (YCTO) is very much similar to CCTO and has the same crystal structure. As per present literature, very few works have been reported on YCTO ceramic. Liang *et al.* (2012) have reported dielectric properties of $Y_{2/3}Cu_3Ti_4O_{12}$ ceramic prepared by solid state reaction method. Li *et al.* (2015) has discussed the phase formation with enhanced dielectric response of YCTO ceramics derived from Sol–Gel process.

High dielectric constant materials need stability in a wide frequency range from the application point of view; especially over 1 MHz. Rare earth doping can be applicable in significant improvement in the working frequency band. In this chapter, rare earth ion was doped into $ACu_3Ti_4O_{12}$ (ACTO) ceramic at A-site to produce $Y_{2/3}Cu_3Ti_4O_{12}$ (YCTO) by the semi-wet route at a relatively low sintering temperature. The phase, microstructure and dielectric properties of this rare earth

based material is characterized with the help of Thermal Analysis (TA), X-ray diffraction (XRD), Scanning Electron Microscopy (SEM), Energy Dispersive X-ray (EDX), Atomic Force Microscopy (AFM) and Transmission Electron Microscopy (TEM). Its dielectric property has been studied in a wide range of frequency 2Hz – 5MHz at different temperature 35-227 $^{\circ}$C.

3.2 RESULTS AND DISCUSSION

3.2.1 Thermal Analysis

Several solid-state reactions accompanied by mass change go through a sequence of steps before yielding a stable product. The ideal temperature for the decomposition of precursor dry powder was determined simultaneously by thermo-gravimetric analysis (TGA), differential thermal analysis (DTA) and differential thermo-gravimetric analysis (DTG). Fig. 3.1 illustrates simultaneous TG/DTA/DTG plots for precursor dry powder of YCTO with a heating rate of 10 $^{\circ}$C min^{-1} in static air from ambient to 1000 $^{\circ}$C. It clearly shows three stages of weight loss with increasing temperature up to 950 $^{\circ}$C. The first significant weight loss occurred at 250, second at 800 and the third one with very small weight loss above 900 $^{\circ}$C. In TGA curve, no further significant weight loss was observed in the temperature range from 950 $^{\circ}$C to 1000 $^{\circ}$C which indicates that the final product forms around 950 $^{\circ}$C. The corresponding DTA or DTG curve shows two strong exothermic peaks near 250 and 850 $^{\circ}$C besides a small peak around 950 $^{\circ}$C. It is also observed that DTG peaks are more intense than DTA peaks. Beyond 950 $^{\circ}$C, no peak was observed which confirms that the final product forms around 950 $^{\circ}$C.

The first weight loss around 250 $^{\circ}$C is due to an exothermic reaction which may be attributed to the elimination of residual water and dehydration of the hydrated gel. The second weight loss at 850 $^{\circ}$C is due to formation of an intermediate complex and this is further supported by the main exothermic peak observed at 850 $^{\circ}$C in the DTA curve. The third weight loss around at 950 $^{\circ}$C is due to an exothermic addition reaction of an intermediate compound with TiO_2 to give the final product $Y_{2/3}Cu_3Ti_4O_{12}$.

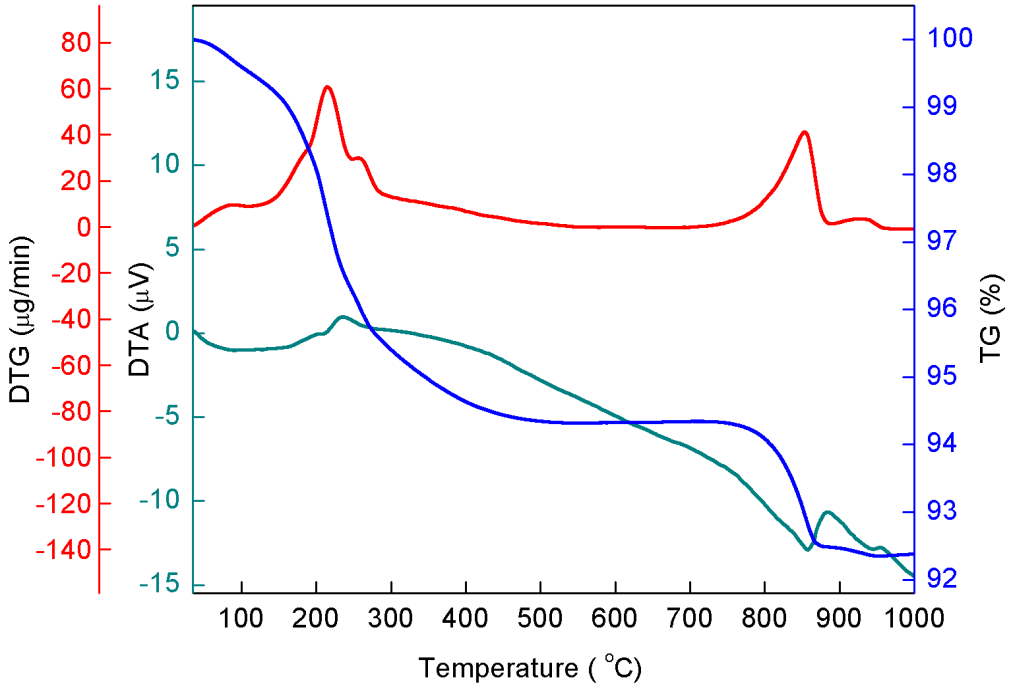

Figure 3.1: DTA/TGA curves for $Y_{2/3}Cu_3Ti_4O_{12}$ (YCTO) dry precursor powder.

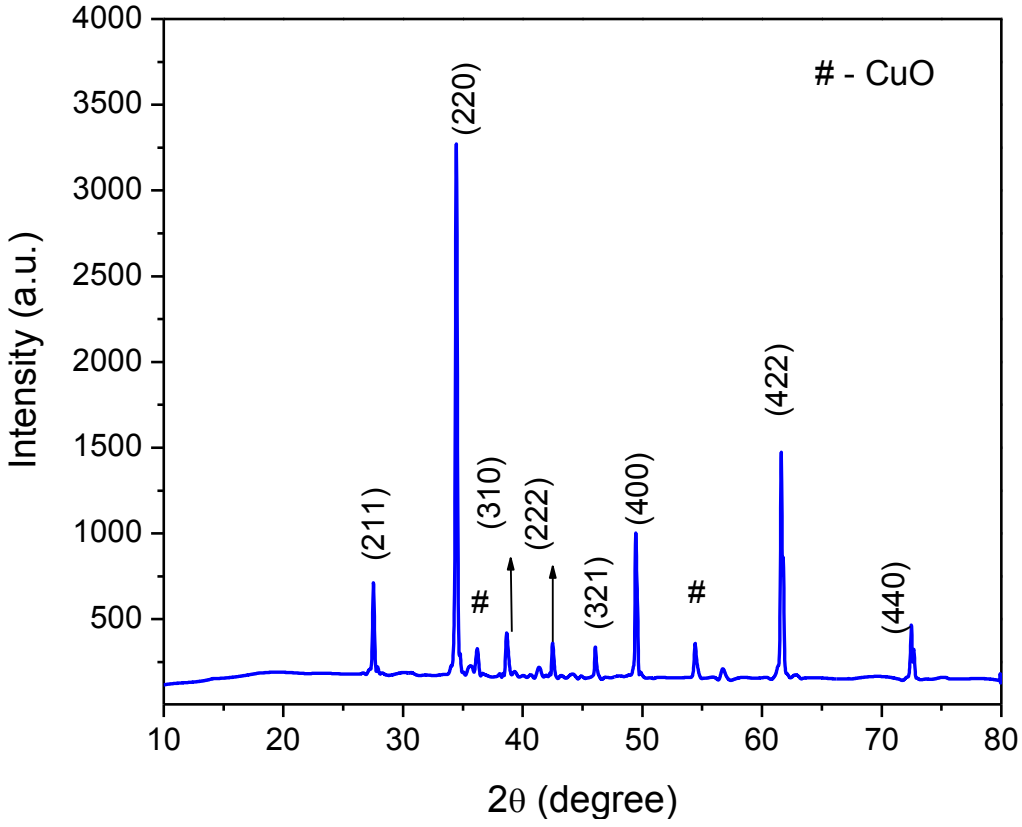

Figure 3.2: XRD patterns of YCTO ceramic sintered at 950 °C for 12h.

3.2.2 X-Ray Diffraction Analysis

XRD pattern of YCTO ceramic sintered at 950 °C for 12h is shown in Fig. 3.2 which clearly shows YCTO phase along with the presence of secondary phase of CuO (JCPDS card no. 80-1917). The main XRD diffraction peaks of YCTO corresponding to (211), (220), (013), (222), (321), (400), (422), (440) planes were found to have good matching with $CaCu_3Ti_4O_{12}$ (JCPDS 75-2188). XRD data were indexed on the basis of a cubic unit cell similar to CCTO. The lattice parameter and unit cell volume of YCTO ceramic were determined by least square refinement method using 'CEL' software. The value of lattice parameter and unit cell volume was found to be 7.4983Å and 421.5833$Å^3$ respectively. XRD pattern shows the presence of split peaks for the reflections 400, 422 and 440. This may be due to the presence of Cu-$K\alpha_2$ along with Cu-$K\alpha_1$ in the X-ray radiations used for diffraction which is supported by the fact that in all these reflections, the intensity of peaks due to Cu-$K\alpha_2$ is close to 50% of the intensity of peak due to Cu $K\alpha_1$ as expected (Culity *et al.*, 2001).

After correction of peak broadening due to instrument, the crystallite size (D) of the YCTO ceramic was determined using the Debye-Scherrer's formula:

$$D = \frac{k\lambda}{\beta \cos\theta} \qquad (3.1)$$

where k is the crystal shape coefficient (k = 0.89), λ is the wave length, β is the corrected full width at half maximum (FWHM) which was obtained by correction of peak broadening due to instrument and θ is diffraction angle. The calculated value of crystallite size for the YCTO ceramic was found to be 68 ± 6 nm and also listed in Table 3.1. The Crystal structure, lattice parameter and unit cell volume of the samples are given in this table.

Table 3.1: Crystal structure, lattice parameter and unit cell volume of $Y_{2/3}Cu_3Ti_4O_{12}$ ceramic

System	Structure	Lattice Parameter (Å)	Unit cell volume $(Å)^3$	Crystallite size (nm) By XRD	Particle Size (nm) by TEM
$Y_{2/3}Cu_3Ti_4O_{12}$	Cubic	7.4983Å	421.5833	68 ± 6	60 ± 20

3.2.3 Scanning Electron Microscopic and Energy Dispersive X-ray Spectroscopic Studies

Fig. 3.3 shows scanning electron micrograph of the fractured surface of YCTO ceramic sintered at 950 $^{\circ}$C for 12h. The SEM micrograph clearly exhibits smooth surfaced grains having a bimodal structure with some pores. The microstructure is dominated by small spherical grains of size 1-2 µm. However, few irregular shaped large grains of size 2-3 µm were also observed. Secondary phases were not seen in SEM micrographs. A similar structure was also observed in the CCTO ceramics sintered at low temperatures (Shao *et al.*, 2006; Pan et al., 2005). The large grain growth is caused due to the presence of liquid phase along the grain boundaries. The amount of CuO phase along this boundary may contribute significant effects to promote the grain growth and densification. It is also established that increase in sintering temperature significantly promotes the grain growth and microstructural densification (Kim *et al.*, 1999; Huang *et al.*, 2002). It is also evident from the Fig. 3.3 that YCTO ceramic shows a high degree of porosity. The calculated value of porosity in YCTO ceramic was found to be 5.6%. The high porosity may be attributed to the formation of oxygen vacancies during sintering. It may also be due to lower sintering temperature. An increase in sintering temperature may lead to the decrease in porosity owing to the grain growth phenomena. Moreover, the porosity also depends upon processing route, the samples prepared by Pechini method and co-precipitation method exhibit a lower extent of porosity than those prepared by other processes at the same sintering temperature (Niwa *et al.*, 2012).The calculated value of the density of YCTO ceramic was found to be 5.99 g/cm^3 which is in agreement with the reported value of undoped YCTO ceramic (Liang *et al.*, 2012).

Fig. 3.4 shows EDX spectra of YCTO ceramic which indicates the presence of Y, Cu, Ti and O elements. Quantitative data for the atomic and weight percentage of the elements present in grain of YCTO ceramic obtained from EDX data were as per expected stoichiometry. It confirms the purity of YCTO ceramic. The atomic percentage of Y, Cu, Ti and O was found to be 3.56, 18.80, 24.65 and 52.99 respectively.

Table 3.2: Percentage of elements in $Y_{2/3}Cu_3Ti_4O_{12}$ (YCTO) sintered ceramic.

Percentage (%)	**Y**	**Cu**	**Ti**	**O**
Weight	8.94	33.76	33.36	23.95
Atomic	3.56	18.80	24.65	52.99

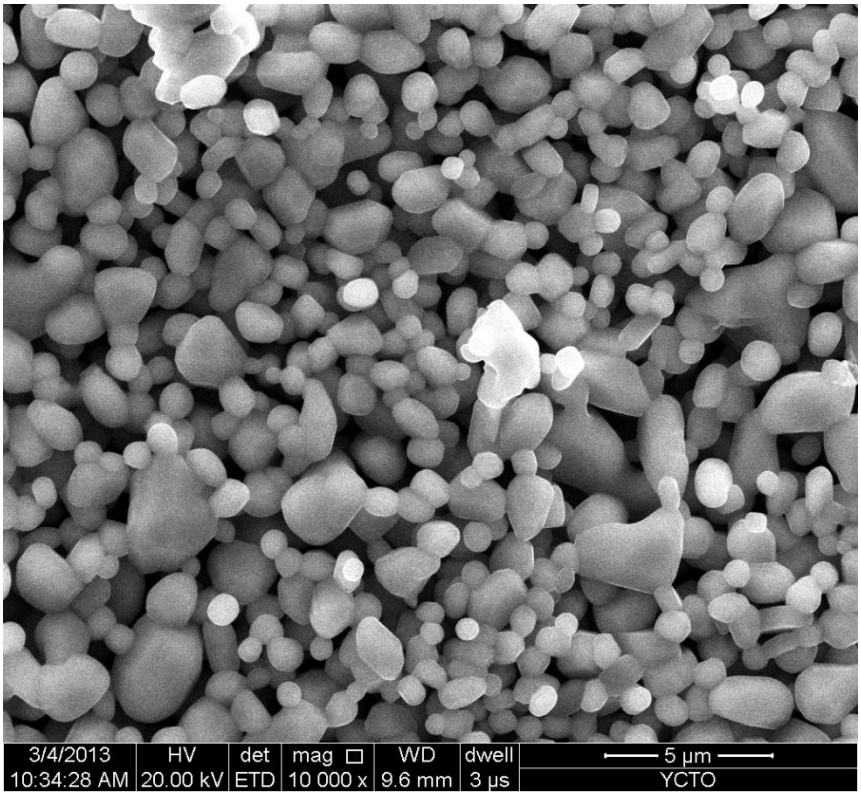

Figure 3.3: SEM micrographs of fractured surface of sintered $Y_{2/3}Cu_3Ti_4O_{12}$ ceramic.

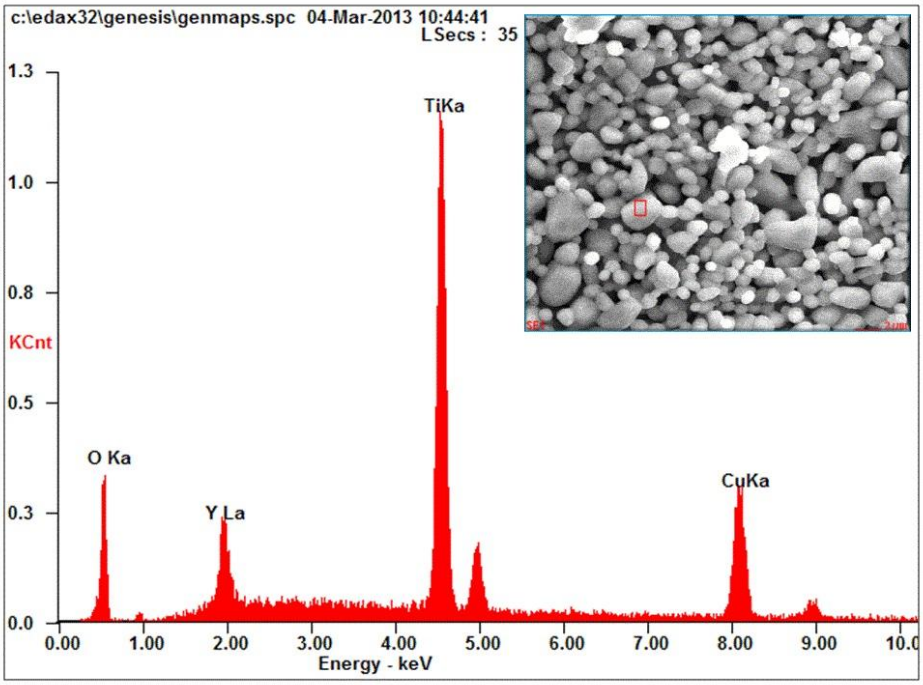

Figure 3.4: EDX spectra of pure $Y_{2/3}Cu_3Ti_4O_{12}$ ceramic sintered at 950 $^{\circ}$C for 12h.

3.2.4 Atomic Force Microscopic Study

The surface topography of $Y_{2/3}Cu_3Ti_4O_{12}$ ceramic was studied with the help of Atomic force microscopy. These images were obtained by a thin film deposition on amorphous glass substrate in a tapping mode. Fig. 3.5(a) depicts the two-dimensional AFM micrograph with 5 µm x 5 µm scan area of YCTO thin film which has a smooth, compact and crack-free surface fully covered by grains. Most of the crystal grains are round and homogeneously distributed upon this surface. The AFM analysis revealed a wider range of particles distribution in the YCTO ceramic. The average grain size estimated by AFM was found to be 59 nm (Fig. 3.6a) and the average diameter of grain was found to be 66 nm (Fig. 3.6b) when the grains were homogeneously mounted over the substrate of an area 0.0041µm^2 (Fig. 3.6c). One can find details of the 2-Dimensional surface roughness of the tested samples by investigation of the amplitude analysis parameters as well as 3-Dimensional roughness by height analysis parameters. The amplitude analysis parameters mainly includes average roughness, root mean square roughness, maximum peak to valley height roughness, ten-point mean height roughness, skewness roughness and kurtosis roughness. Through the

roughness parameters, the surface condition of the entire measured length or area will be evaluated in terms of peak and valley (Raposos *et al*., 2007).

Based upon the statistical study of total 324 grain ensembles within the length 3.533 μm and scanning area 5 μm × 5 μm for two-dimensional AFM image of surface of YCTO thin film, the value of average roughness (R_a) and Root mean square roughness (R_q) was estimated to be 1.854 and 2.288 nm. The average roughness gives the deviation of the calculated mean height over the measured area while Root mean square roughness demonstrates the standard deviation of the surface height over the measured area. The Maximum peak to valley height roughness (R_t) which summarizes the total roughness of the measured area was found to be 10.559 nm whereas the Ten-points mean height roughness (R_z) shows the mean height difference between the average of the five highest peaks and the five lowest valleys in the evaluation surface was found to be 8.328 nm.

The functional parameters such as skewness (R_{Sk}) and kurtosis (R_{Ku}) moments are used to measure the asymmetry and the flatness, respectively. The Skewness roughness (R_{sk}) is used to measure the profile symmetry of the mean line was found to be 0.0136 about nearly to zero, while kurtosis roughness (R_{ku}) is used to measure the surface sharpness which is in fact, the distribution of the spikes above and below the mean line was found to be 2.641 which is less than 3. Apart from the average roughness, the lower positive values of skewness roughness (R_{sk}) imply for the smoothness of surface with predominant peaks while higher positive value for kurtosis roughness (R_{ku}) indicating that the surface of scanned area of YCTO thin film is slightly bumpy in nature due to the appearance of low number of high peaks and low valleys on the surface. It is more evident from the 3D image (Fig. 3.5 C). As kurtosis value is less than three, such distribution curve is called Platykurotic which is usually characterized by relatively few high mountain and valley.

Fig. 3.5(b) shows the grains and grain boundary regions in YCTO thin film. It exhibits compact structure with granular morphology, buffer layer, plates like grains and clear grain boundary. Fig. 3.5(c) exhibits its three-dimensional surface morphology exhibits several peaks corresponding to grain with compact structure. Based upon the statistical study of total 2.5×10^6 grains within the scanning area 5 μm × 5 μm and sampling and evaluation area 25.019 μm^2 for the three-dimensional

AFM image of YCTO thin film surface, the value of average roughness (Sa) and Root mean square roughness (Sq), maximum peak to valley height roughness (S_z) and 10-points mean height roughness (S_{10z}) was estimated to be 1.517, 1.978, 26.979 and 21.085 nm, while skewness S_{ku} and kurtosis (S_{sk}) was found to be 0.473 and 5.789. The Kurtosis value of 3D AFM-image is of thin film surface of YCTO is quite interesting, as its value is greater than 3, confirming the distribution curve to be Leptokurtoic which in turn, is characterized by many high peak but low valley. It is also agreement with the 3D AFM-image. 3D surface analysis refines the data and findings obtained in 2D mode in a more accurate way.

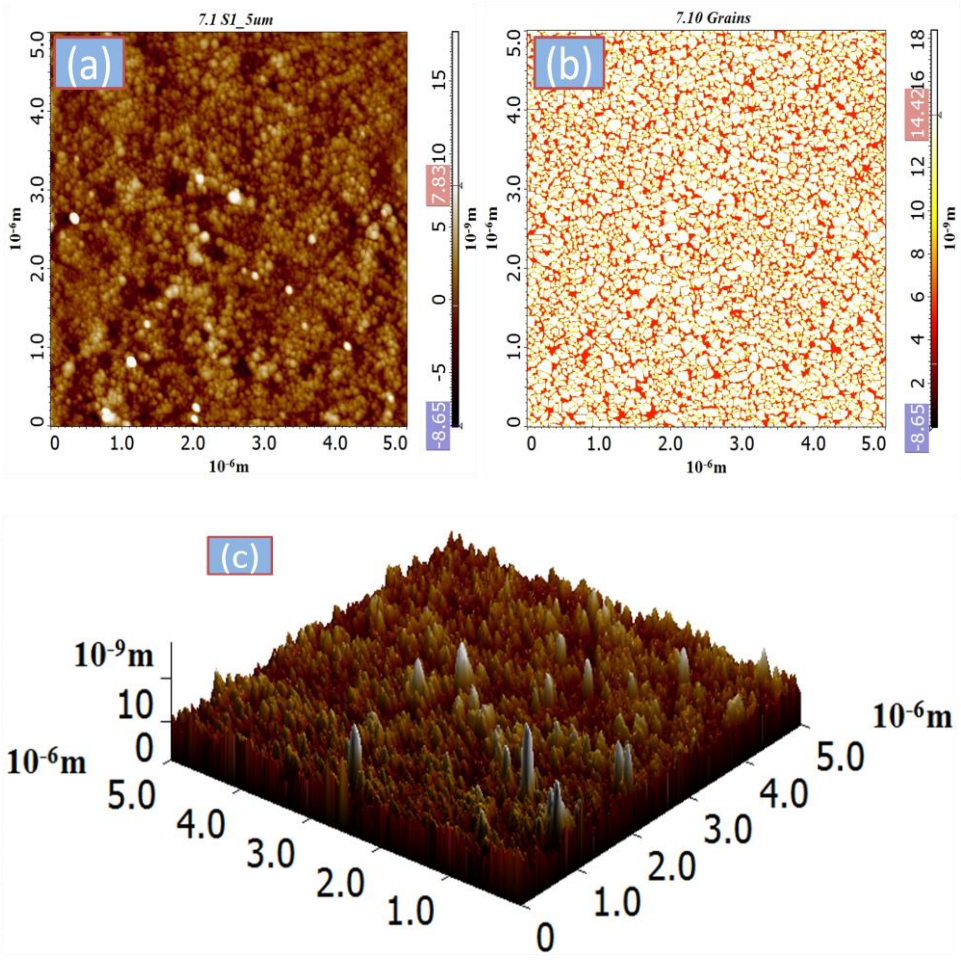

Figure 3.5: (a) 2- dimensional AFM micrograph of thin film (b) 2-dimensional AFM micrograph showing grain boundary (c) 3- dimensional AFM micrograph of sintered $Y_{2/3}Cu_3Ti_4O_{12}$ ceramic.

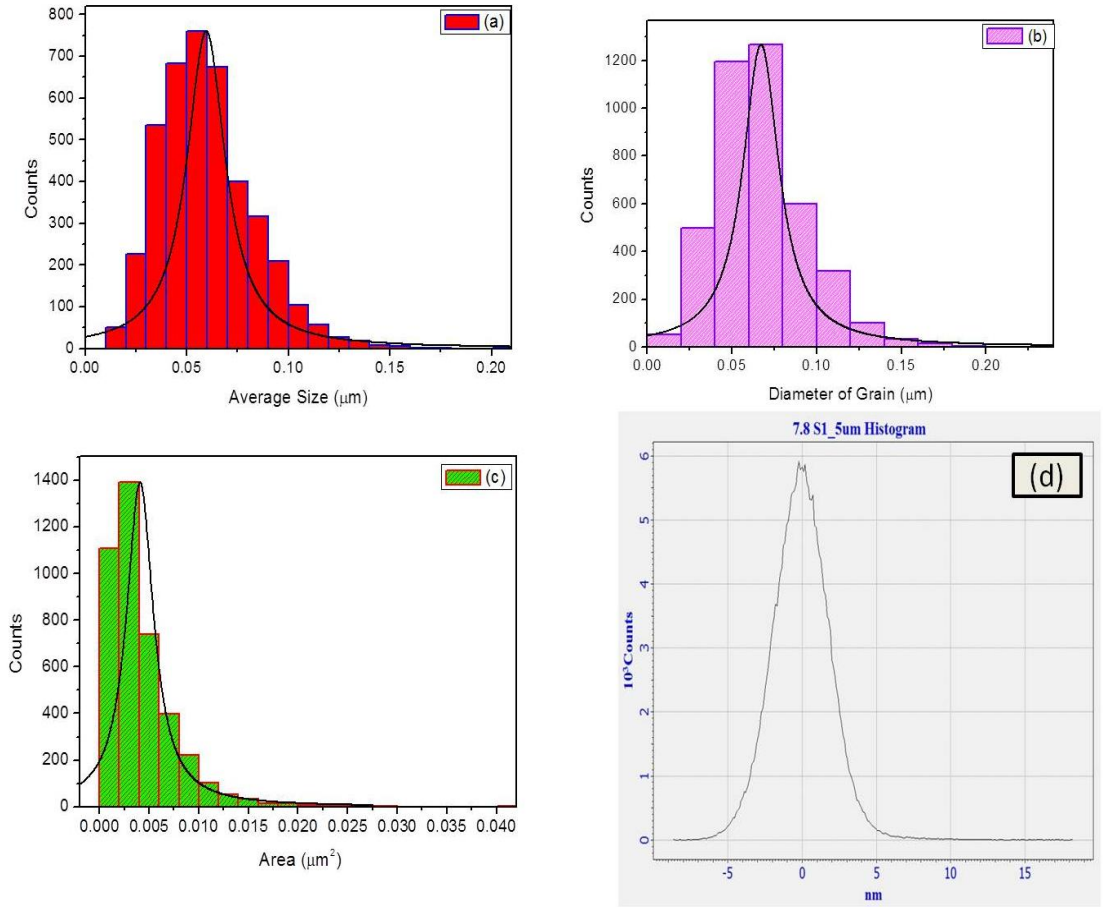

Figure 3.6: Different histograms for sintered $Y_{2/3}Cu_3Ti_4O_{12}$ ceramic exhibiting (a) Average size (b) Diameter of grains (c) Area of grains and (d) Average 3- dimensional roughness.

The surface roughness parameters of the tested sample in 2D and 3D AFM study of YCTO thin film, deduced with the help of NOVA software are summarized in Table 3.3.

Table 3.3: The surface roughness parameters of YCTO thin film obtained by 2D- and 3D- AFM-image mapping.

Details of Roughness	**Parameters**	
	2D (Amplitude)	**3D (Height)**
Average /Arithmetic	1.854	1.517
Root Mean Square	2.288	1.978
Maximum peak to valley height roughness	10.559	26.979
Ten-points mean height roughness	8.328	21.085
Skewness	0.0136	0.473
Kurtosis	2.641	5.789

3.2.5 Transmission Electron Microscopic Study

The bright field TEM image of YCTO ceramic sintered at 950 $^{\circ}$C for 12h is presented in Fig. 3.7(a). The TEM image confirms that the YCTO ceramic consists of crystalline particles of faceted shape. The particles are well dispersed with some agglomeration. The average size of the particles is 60 ± 20 nm which is in agreement with XRD results. It is reported in literature that in case of small nano particles both results coincide (Carter *et al.*, 2009). The corresponding selected area electron diffraction (SAED) pattern of TEM image is shown in Fig. 3.7(b). The presence of few clear rings in SAED pattern again confirms the formation of the polycrystalline phase of thermodynamically stable YCTO ceramic. TEM diffraction pattern was indexed on the basis of a body-centered cubic perovskite structure. The lattice parameter calculated from the electron diffraction pattern is also in agreement with those measured from the XRD pattern. The zone axis of the selected area electron diffraction (SAED) of the YCTO ceramic was calculated and was found to be $[\overline{1}, 3, \overline{1}]$.

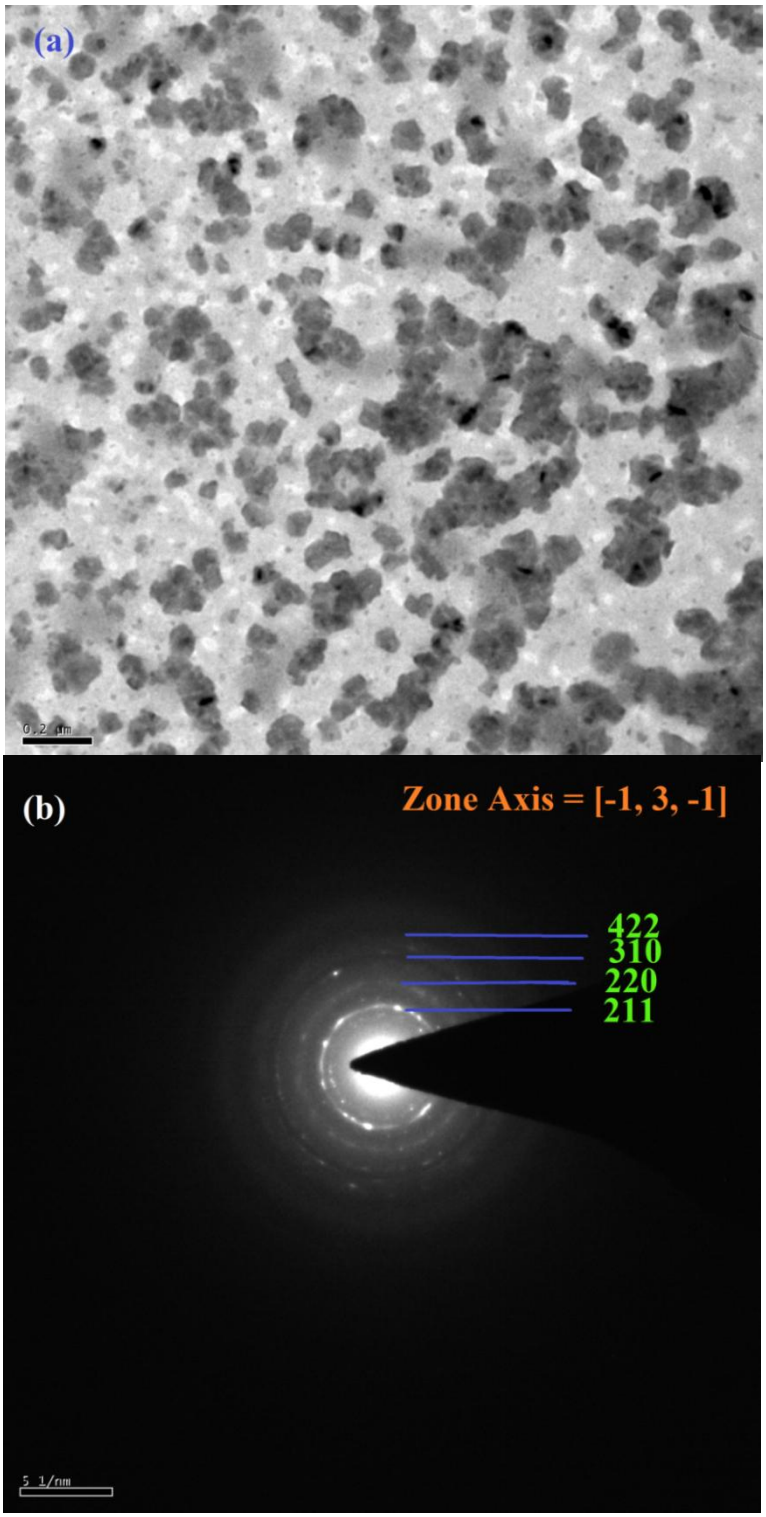

Figure 3.7: (a) Bright field TEM micrographs (b) Corresponding Selected Area Electron diffraction Pattern of sintered $Y_{2/3}Cu_3Ti_4O_{12}$ ceramic

3.2.6 P-E Loop measurement

The origin of polarization and ferroelectric behavior of ceramic may be justified with the help of polarization electric (P-E) Loop tracer technique. PE hysteresis loop is related to its energy storage ability and it displays significant material property of dielectric materials. This loop can be discussed in terms of three important parameters viz. remnant polarization (P_r), saturated polarization (P_s) and coercive field (E_c) under the external electric field. The PE hysteresis loop obtained at 308 K for $Y_{2/3}Cu_3Ti_4O_{12}$ ceramic is shown in Fig. 3.8. The value of remnant polarization (Pr), saturation polarization and coercivity (E_C) are found to be 0.196μC/cm^2, 0.951μC/cm^2 and 0.437kV/cm, respectively. This may be due to the alignment of domains present in the ceramic which increases with temperature in absence of electric field. Another reason may be the display of high dielectric constant phenomenon, contributing significantly to the relaxor-ferroelectric behavior (Raya *et al.*, 2013).

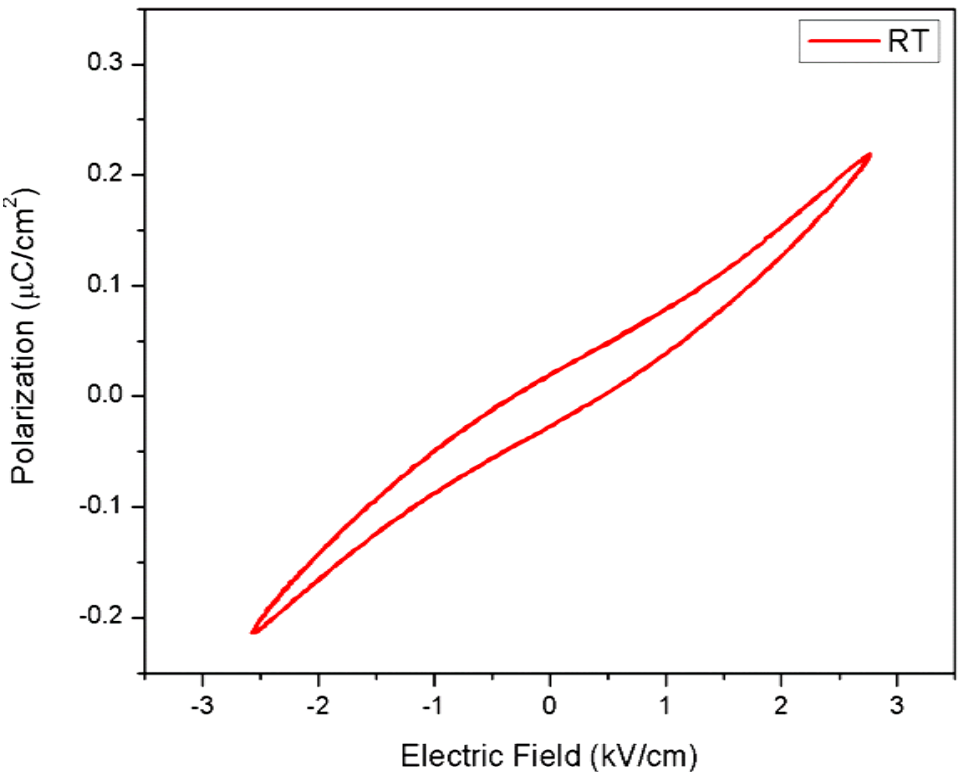

Figure 3.8: P-E hysteresis loop of $Y_{2/3}Cu_3Ti_4O_{12}$ ceramic at 308 K.

3.2.7 Dielectric and Electric Behavior

Plots of dielectric constant (ε′) and dielectric loss (tan δ) as a function of temperature at a few selected frequencies for YCTO ceramic are shown in Fig. 3.9. It is clear from Fig. 3.9(a) that the variation of ε′ with temperature at 100 Hz shows a step-like increase from a low value 8434 at room temperature (308 K) to a high value 12849 at 353 K and then it decreases to 1072 at 425 K. YCTO ceramic exhibits almost frequency independent dielectric constant above 450 K. It is reported in the literature that above the room temperature a broad dielectric peak appears from 350 K to 425 K which gets suppressed further at higher frequencies. It shows relaxor behaviour in the ceramic which is usually characterized by diffuse phase transition and strong relaxational dispersion in dielectric constant and loss tangent (tan δ) which may be due to thermally activated relaxation (Cross 1994).

It is noted from the Fig. 3.9(b) that the value of tan δ increases first, attains a maxima and then decreases smoothly to a lower value. At 100 Hz, tan δ increases from a value of 3.4 at 308 K, attains a maximum of 5.4 at 365 K and then it decreases abruptly to a value 0.46 at 450 K. Such a trend is again a direct evidence for Maxwell-Wagner relaxation phenomena. The dielectric loss of YCTO ceramic at 350 K was found to be 4.9, 4.0, 2.2 and 0.79 at 0.10, 1.0, 10 and 100 kHz respectively. It is also observed that dielectric loss of YCTO ceramic was found to be higher than undoped CCTO ceramic at 350 K synthesized by semi wet route (Li *et al.*, 2004).

The presence of dispersion peaks in the figures, ε′-T and tan δ-T, below 425 K and at lower frequencies (i.e. less than 1 KHz) supported the presence of Maxwell-Wagner type relaxation behavior in the ceramic. The presence of low frequency relaxation may be attributed to the occurrence of space charge polarization arising at the interface of grain and grain boundary which has a large difference in their electrical conductivity.

The diffuse phase transition may be due to micro-heterogeneities operative due to random occupation of A and B sites by different ions in ABO_3 type perovskites. Such a heterogeneous distribution of cations leads to different state of polarization and distribution of relaxation time in different regions. This is causes dielectric maxima to get diffuse. For its verification, ε^{-1} is plotted against temperature

according to the relation proposed by Uchino and Namura for the materials which show ferroelectricity at room temperature. The diffuse phase transition phenomena in YCTO ceramic can be justified by fitting of ε′ in the variable power law at room temperature

$$\frac{1}{\varepsilon'} = \frac{1}{\varepsilon'_m} + \frac{(T - T_m)^{\gamma}}{C} \tag{3.2}$$

where ε′ and ε'_m is the dielectric constant and its maximum value, respectively. The value of power factor γ close to 1 suggests normal ferroelectrics, while close to 2 suggests relaxor ferroelectrics. The curve fitting results corresponding to YCTO is shown in Table 3.4.

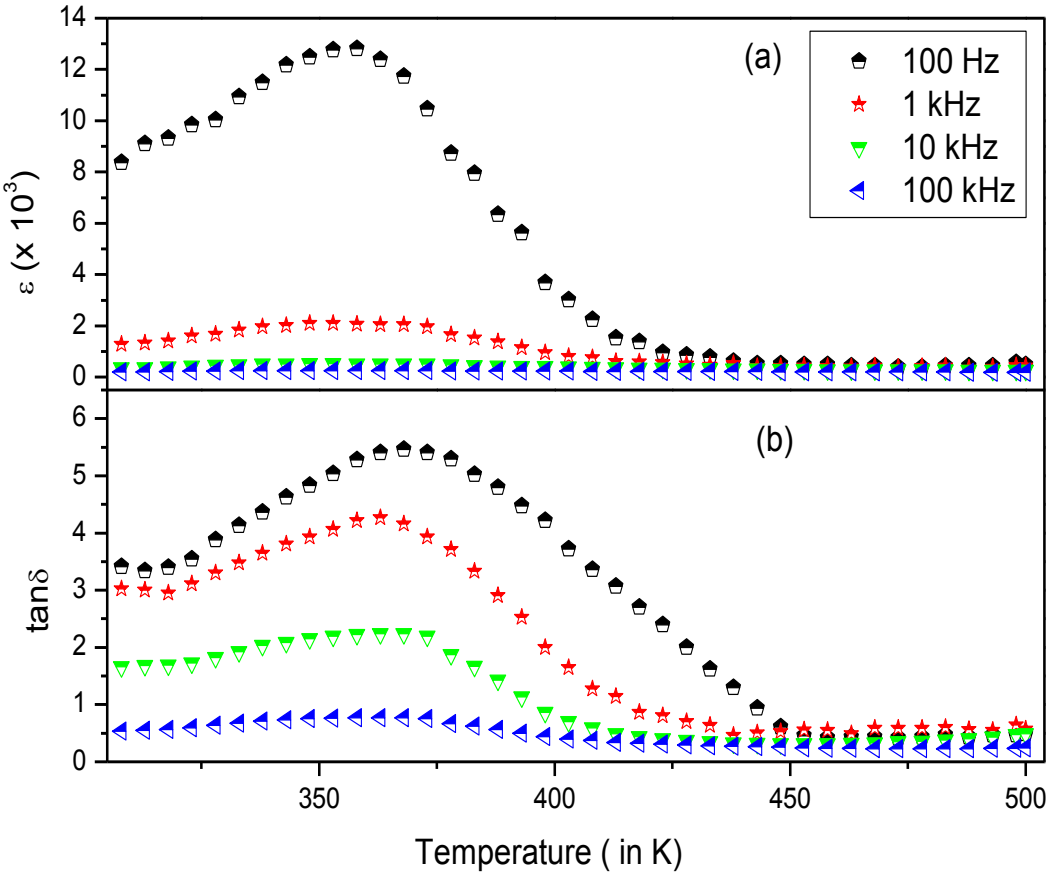

Figure 3.9: Variation of (a) dielectric constant (ε′) and (b) loss tangent (tan δ) with temperature at a few selected frequency for sintered YCTO ceramic.

The power extent γ arises from 1.72 to 1.87 which clearly indicates the presence of diffuse phase transition in YCTO ceramic, a clear confirmation of relaxor ferroelectric behavior of the ceramic below 425K. The slowing down of the relaxation process can be attributed to the evolution of an exponential distribution of the relaxation time.

Table 3.4: The curve fitting results of variable power law for $Y_{2/3}Cu_3Ti_4O_{12}$ ceramic.

Frequency	T_m **(K)**	$1/\ _m$ **(10^{-5})**	**γ**
100 Hz	357	7.48	1.72
1 kHz	358	3.15	1.87

Fig. 3.10 illustrates the frequency dependence of ε′ and ε″ of sintered YCTO ceramic at a few selected temperature. The value of ε′ for YCTO ceramic was found to be 8434 at 308 K and 100 Hz, which is much higher than the value reported earlier (Subramanian *et al.*, 2000). It is also evident that the value of dielectric constant (ε′) decreases steeply in the lower frequency range whereas in the higher frequency range it decreases slowly as shown in the inset. The decrease in dielectric constant with frequency may be due to the space charge accumulation at the interface which leads to polarization of the ionic medium and hence increases the value of ε′. In high-frequency regions, the periodic reversal of the field takes place so rapidly that there is no charge accumulation at the interface, resulting in a constant ε′ value (Tareev 1975).

The direct evidence for relaxor behavior of YCTO arises from the frequency dependence of the imaginary part of dielectric constant (ε″) as shown in Fig. 3.10(b). It is apparent from the figure that dielectric relaxation was also encountered around 10^5 - 10^6 Hz. These relaxation peaks, which are clearer from the inset, shift towards higher frequency region with grain boundaries. The sharp peaks also support the presence of Maxwell -Wagner relaxation.

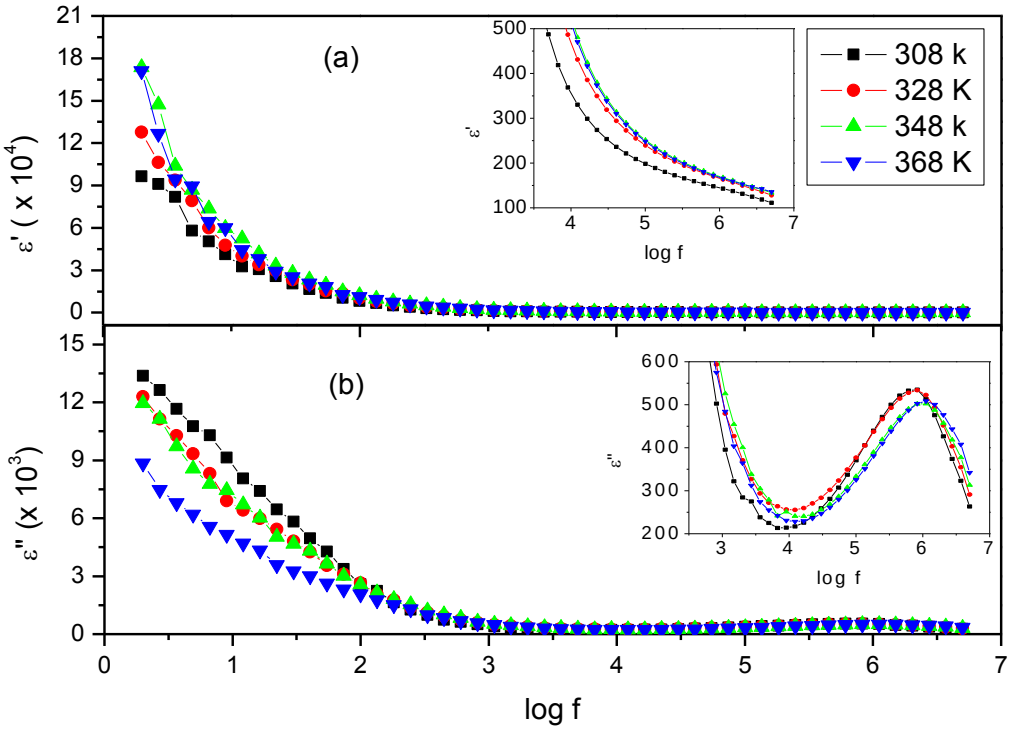

Figure 3.10: Variation of (a) real part of dielectric constant (ε′) and (b) imaginary part of dielectric constant (ε″) with frequency at different temperature for sintered YCTO ceramic.

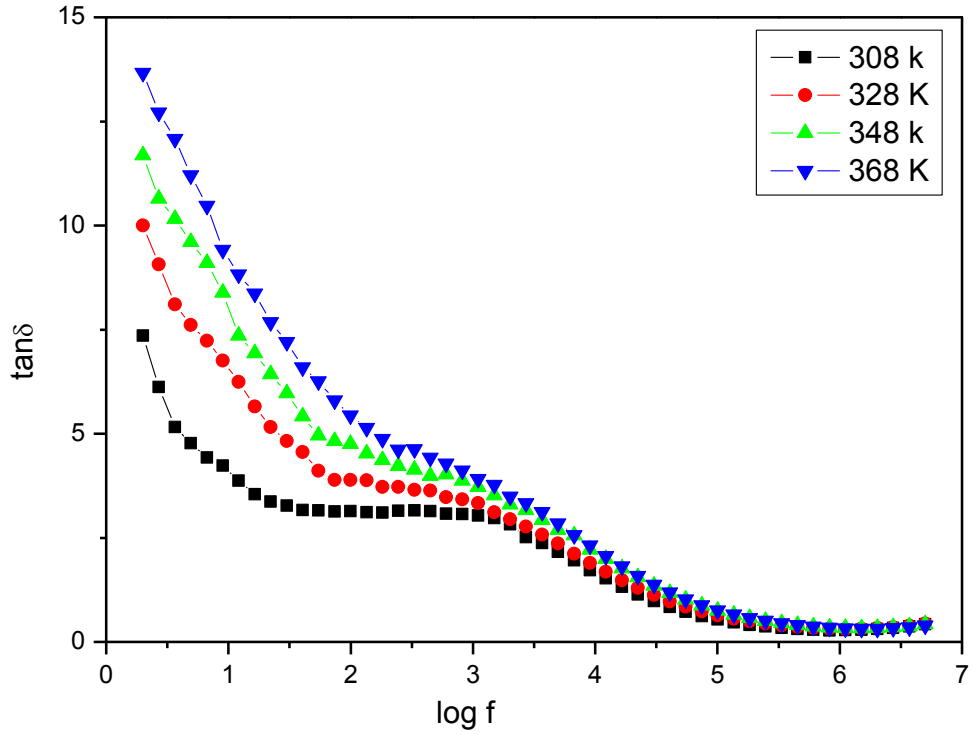

Figure 3.11: Variation of tanδ with frequency at different temperatures for sintered YCTO ceramic.

It is also reported in the literature that ε″ exhibits a maximum at ω=1/τ where the oscillating charges are coupled with the oscillating field and absorbs a maximum electrical energy.

Fig. 3.11 shows the variation of loss tangent (tan δ) with frequency. It is evident from the figure that the value of tan δ decreases with increase in frequency in lower frequency region while it decreases smoothly in the higher frequency region. Peaks were observed for all the measured temperature at 1 kHz. The dielectric loss of YCTO ceramic was found to be 1.5 to 2.04 at 10 kHz from 308 to 428 K.

3.2.8 Impedance Spectroscopic studies

Investigation of dielectric dispersion and formation of a barrier layer in YCTO ceramic may be confirmed by complex plane impedance (Z*) and complex plane electric modulus (M*) spectroscopic studies. Information regarding the simultaneous occurrence of multi-polarisation processes and their relaxation conditions can be obtained by these studies (Veith *et al.*, 2009).

The effective contributions of grains, grain-boundaries and electrode interface specimen to the total resistance and capacitance can also be determined by impedance spectroscopy, which correlates the electrical behavior of the sample to its microstructure. The concept of the simplest equivalent circuit containing a series of three parallel RC elements can be applied to $ACu_3Ti_4O_{12}$ type of ceramic (Sinclair *et al.*, 2002; Mitsugi *et al.*, 2007). For all the three contributions (Fig. 3.12), three circular arcs can be obtained at a lower temperature (below 273 K).They may have their centres on or below the real axis Z′ depending on whether there is a single relaxation time for each of the above processes, or there is distribution of relaxation time. The non-zero intercept of the arc passing through the origin on Z′ axis will give the grain contribution (**R_g**) in high-frequency range while that of another arc in the lower frequency range will represent the contribution of grain boundary (R_{gb}) and electrode effect (R_{el}). Impedance can be calculated from the following equations:

$$Z^* = \frac{1}{R_g^{-1} + i\omega C_g} + \frac{1}{R_{gb}^{-1} + i\omega C_{gb}} = Z' - iZ'' \qquad (3.3)$$

where, $$Z' = \frac{R_g}{1+(\omega R_g C_g)^2} + \frac{R_{gb}}{1+(\omega R_{gb} C_{gb})^2} \quad (3.4)$$

and $$Z'' = R_g\left[\frac{\omega R_g C_g}{1+(\omega R_g C_g)^2}\right] + R_{gb}\left[\frac{\omega R_{gb} C_{gb}}{1+(\omega R_{gb} C_{gb})^2}\right] \quad (3.5)$$

where Z^* , Z' and Z'' are complex impedance, the real part of impedance, the imaginary part of impedance, respectively.

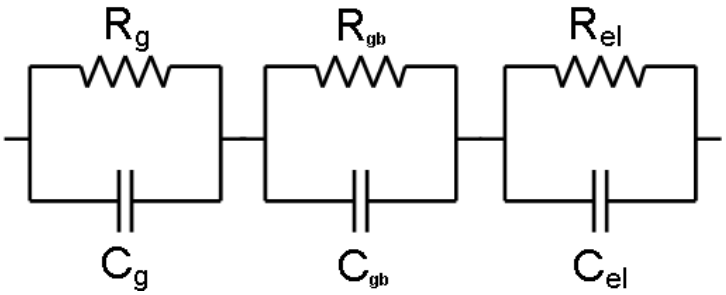

Figure 3.12: The simplest equivalent circuit is a series of network of three parallel RC elements.

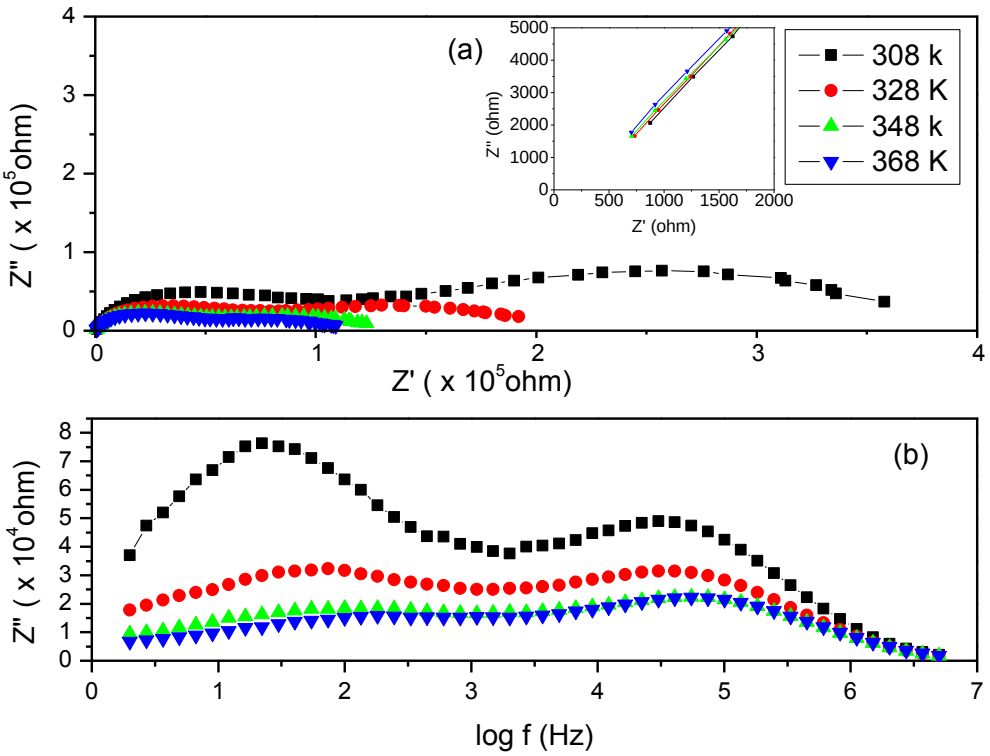

Figure 3.13: (a) Complex impedance plane plots (Z′ vs Z″) (b) Variation of Z″ with frequency at a few selected temperatures for sintered YCTO ceramic.

The complex impedance plot of YCTO ceramic sintered for 12h at a few selected temperatures is shown in Fig. 3.13(a). The figure clearly reveals the presence of two semi-circular arcs with different intercepts which may be due to the grain boundary and electrode surface effects. The inset figure shows the data in the high-frequency region. On extrapolation, the intercept on Z′ axis is not found to be close to zero suggesting an existence of another semi-circle in high-frequency region beyond the measuring frequency range. The non-zero intercepts on Z′ axis give the grain resistance values which are listed in Table 3.5. It is also observed that with increasing temperature the size of arc (i.e. resistance) decreases. The resistance of grain boundaries at different temperatures was also calculated from the arc and is shown in Table 3.5. The arcs for grains at high frequency get suppressed due to high value of grain boundary resistance which is usually observed for internal barrier layer capacitance (IBLC), a characteristic of semiconducting grain with insulating grain boundary. The electrode resistance appears at all measured temperatures which may be due to electrode polarisation effects present in the YCTO ceramic. Thus, the dielectric property of YCTO ceramic is due to the combined effect of grain and grain boundary. From the Table 3.5, it is inferred that the resistance of grain boundary is very high in comparison to those of grains and resistance of both decreases with increasing temperature.

Table 3.5: Calculated values of resistances and capacitances of grain and grain boundary at a few temperatures for sintered $Y_{2/3}Cu_3Ti_4O_{12}$ nano- ceramic.

Temp. (K)	**R_g(Ω)**	**R_{gb}(Ω)**	**C_g (pF)**	**C_{gb} (nF)**
308	354.33	1.27×10^5	-	9.13
328	291.55	0.58×10^5	-	9.22
348	266.17	0.48×10^5	-	9.25
368	199.12	0.27×10^5	-	9.29

The variation of the imaginary part of impedance Z'' with frequency at a few selected temperatures is shown in Fig. 3.13(b). It demonstrates the appearance of two relaxation peaks at all measured temperatures, one at around 75 Hz and the other around 10 kHz. The relaxation peaks at a lower frequency region may be due to the electrode effects whereas at a high frequency region it may be due to grain boundary effects. These peaks were suppressed and slightly shifted to a high-frequency region on increasing temperature which confirming the existence of a temperature-dependent Maxwell-Wagner dielectric relaxation. It is also noticed that the inflection point in the impedance plots is the same as that of relaxation peaks in the corresponding ε'' vs log f plot (Fig. 3.10 b). This gives a clear evidence for the occurrence of Maxwell-Wagner relaxation in YCTO ceramic.

3.2.9 Modulus Spectroscopic studies

As an alternative approach, modulus spectroscopic studies was also adopted for exploring the electrical properties of YCTO material and to magnify any other polarization effects present in the sample which may be unidentifiable or superimposed on each other's in impedance spectroscopic studies, probably due to different relaxation time constants, The different parameters of dynamical aspects of electrical transport phenomena such as carrier or ion hopping rate, conductivity relaxation time, etc. can be interpreted also by this technique. The representation of data in terms of Modulus suppresses the unwanted effects of extrinsic relaxation, is often used in the analysis of dynamic conductivities of some ionic conducting ceramics, with the same time, it can discriminate against electrode polarization and grain boundary conduction processes. Sinclair and West (2002) suggested the combined usage of impedance and modulus spectroscopic plots to rationalize the dielectric properties. It is quite obvious that complex impedance plane plots of Z'' vs Z' are significant in the determination of the dominant resistance of any ceramic, but are insensitive to the smaller values of resistances. Similarly, complex modulus plots are useful in determining the smallest capacitance.

For an electrically heterogeneous system, the two parallel RC circuits can be represented by a Schottky junction in such case, the complex modulus response can be given by:

$$M^* = M' + iM'' \tag{3.6}$$

$$M' = \frac{\varepsilon'}{(\varepsilon')^2 + (\varepsilon'')^2} \tag{3.7}$$

$$M'' = \frac{\varepsilon''}{(\varepsilon')^2 + (\varepsilon'')^2} \tag{3.8}$$

The presence of long-range conduction phenomenon, as well as different types of microscopic processes responsible for localized dielectric relaxations in YCTO ceramics was investigated separately by modulus spectroscopic studies. Impedance data were re-plotted in modulus formalism to confirm the presence of grain and grain boundary effects. However, no significant information was obtained by the Cole-Cole plot between M′ and M″ as shown in Fig. 3.14(a). It justifies only a poly-dispersive nature for the dielectric relaxation at low frequencies. Such observation may be correlated to the lack of resorting force governing the mobility of charge carriers under the action of an induced electric field. This behaviour supports the long-range conduction phenomenon. To explain the modulus spectra of YCTO ceramic, the variation of the imaginary part of electric modulus M″ is plotted against frequency at few selected temperature and is shown in Fig. 3.14(b). It confirms the presence of well-defined relaxation phenomena consisting of two relaxation peaks. The peak in the higher frequency region may be due to grain boundary while lower frequency region may be due to electrode effect. Modulus results so obtained also coincide with impedance results. The capacitance of grain boundary was calculated from the plot and recorded in Table 3.5. The values of capacitance were found to be nearly constant at different temperatures which are confirmed from the same peak height of the grain boundary with increasing temperature as shown in the Fig. 3.14(b). Further, the relaxation peaks shifts to higher frequency region with increasing temperature which gives a direct evidence of temperature dependent relaxation. This behaviour also suggests that the dielectric relaxation is thermally activated in which hopping mechanism of charge carrier dominate intrinsically (Dhawajam *et al.*, 2012).

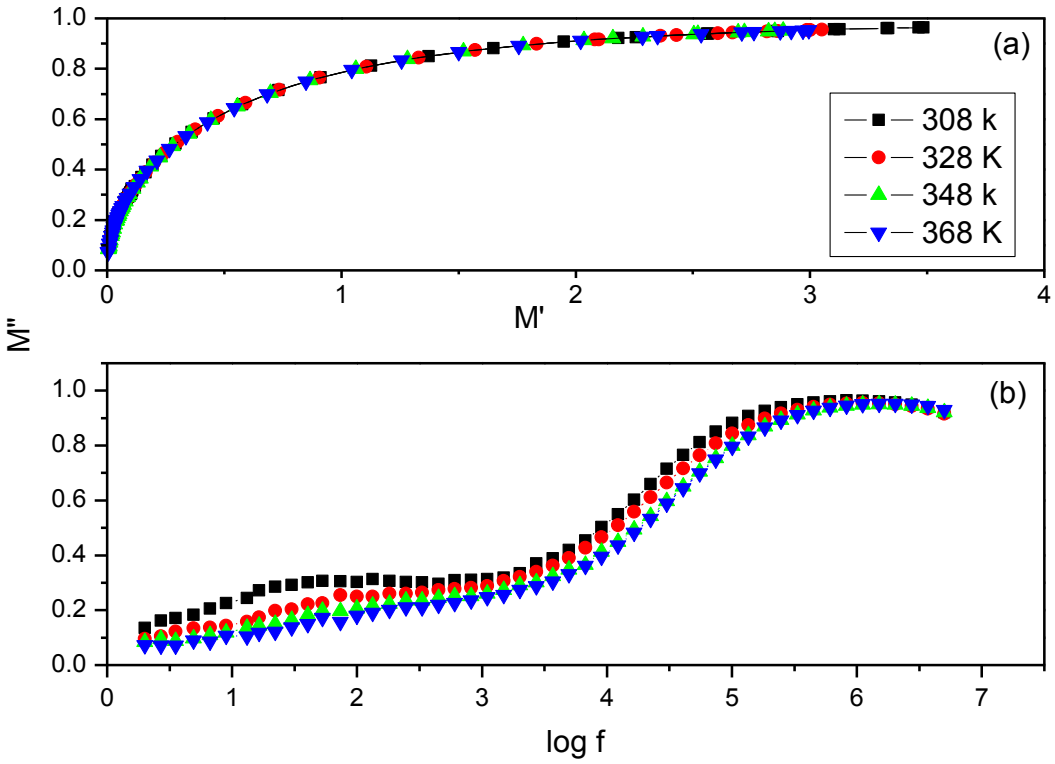

Figure 3.14: (a) Electric modulus plots (M′ vs M″) (b) Variation of M″ vs frequency at a few selected temperature for sintered YCTO ceramic.

3.3 CONCLUSION

Nano-sized $Y_{2/3}Cu_3Ti_4O_{12}$ ceramic was synthesized by the semi-wet route using metal nitrate solution and solid TiO_2 in powder form. XRD confirmed YCTO phase formation along with the presence of a minor secondary phase of CuO. The particle size of the YCTO ceramic was found to be 68 ± 6 nm by XRD and 60 ± 20 nm by TEM studies which are in good agreement. Dielectric constant and tangent loss are temperature independent in higher frequency region but temperature dependent in low-frequency region. The impedance of YCTO ceramic shows two significant contributions associated with the grain boundaries and electrode effect. The grain-boundary resistance appears as a significant contribution at a higher temperature. The electrode resistance appears at a lower temperature due to electrode polarization. Modulus analysis of YCTO ceramic confirmed the presence of Maxwell-Wagner type of relaxation which is temperature dependent.